

Parity recognition of blade number and manoeuvre intention classification algorithm of rotor target based on micro-Doppler features using CNN

WANG Wantian, TANG Ziyue, CHEN Yichang*, and SUN Yongjian

Department of Early Warning Technology, Air Force Early Warning Academy, Wuhan 430019, China

Abstract: This paper proposes a parity recognition of blade number and manoeuvre intention classification algorithm of rotor target based on the convolutional neural network (CNN) using micro Doppler features. Firstly, the time-frequency spectrograms are acquired from the radar echo by the short-time Fourier transform. Secondly, based on the obtained spectrograms, a seven-layer CNN architecture is built to recognize the blade-number parity and classify the manoeuvre intention of the rotor target. The constructed architecture contains a leaky rectified linear unit and a dropout layer to accelerate the convergence of the architecture and avoid over-fitting. Finally, the spectrograms of the datasets are divided into three different ratios, i.e., 20%, 33% and 50%, and the cross validation is used to verify the effectiveness of the constructed CNN architecture. Simulation results show that, on the one hand, as the ratio of training data increases, the recognition accuracy of parity and manoeuvre intention is improved at the same signal-to-noise ratio (SNR); on the other hand, the proposed algorithm also has a strong robustness: the accuracy can still reach 90.72% with an SNR of -6 dB.

Keywords: micro-Doppler, convolutional neural network (CNN), parity recognition of blade number, manoeuvre intention classification.

DOI: 10.23919/JSEE.2020.000062

1. Introduction

With the rapid advancement of radar intelligence, effective recognition and classification of aircraft targets become more and more significant in the next-generation radar [1,2]. Feature extraction is the core procedure of radar target recognition and classification [3], and micro-Doppler features are widely used in rotor target classification [4,5]. For example, the micro-Doppler signature and cadence-

velocity diagram are merged as a new image to realize drone classification based on the convolutional neural network (CNN) [6]. In [7], several physically interpretable features are extracted to recognize human activities. However, most of the existing references on target classification are about the classification of target types and models [8,9]. At present, there is no study on the problem of target manoeuvre intention classification. The micro-Doppler feature can represent not only the difference of dynamic components between different types of targets but also the difference between different manoeuvre intentions of the same target [10]. Taking a helicopter in the rising state as an example, its dynamic components will generate a Doppler modulation with an increasing frequency on the echo; conversely, when the target is falling, its dynamic components will generate a Doppler modulation with a decreasing frequency on the echo. Extraction of the blade characteristic [11] and manoeuvre intention information of a rotor target from micro-Doppler features [12] will be widely used in airspace surveillance and remote sensing applications.

Recently, the CNN is one of the most frequently used methods in intelligent classification algorithms [13–17]. Chen et al. proposed a multistatic CNN algorithm based on micro-motion features to improve the classification probability [18,19]. In [20], a contextual deep CNN (DCNN) was proposed to clarify the hyperspectral image which is different from the other existing networks because of not only the deeper and wider architecture but also the local optimization. In addition, on the basis of raw micro-Doppler spectrograms, the DCNN was utilized to realize human activity recognition without any explicit features extraction [21]. However, the research on the application of the CNN to the artificial target is less and difficult. In this paper, inspired by intelligent classification algorithms, we propose an effective CNN architecture for the parity recog-

Manuscript received July 05, 2019.

*Corresponding author.

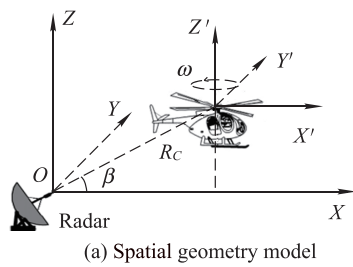
This work was supported by the National Natural Science Foundation of China (61901514) and the Young Talent Program of Air Force Early Warning Academy (TJRC425311G11).

nition of blade number and manoeuvre intention classification of a rotor target. First, time-frequency spectrograms are acquired by the short-time Fourier transform (STFT) based on the analysis of the target echo model [22]. Moreover, a CNN architecture with seven layers is built to recognize the blade number parity and classify the manoeuvre intention of the rotor target, which consists of three convolutional layers (CLs), two down sampling layers (DSLs), and two full connection layers (FCLs). In addition, the activation function of the leaky rectified linear unit and the dropout layer are carried out in the constructed architecture to accelerate the convergence of the architecture and avoid over-fitting. Different from the existing CNN-based methods where the CNN algorithms are mainly used for target type classification, this paper applies the CNN to the field of rotor target manoeuvre intention classification.

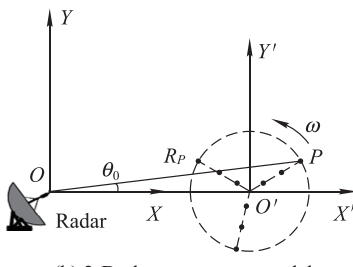
2. Background

2.1 Signal model

Assume that there is a scene of radar detection of a rotor target, and Fig. 1(a) shows the spatial geometry model. R_C refers to the initial distance between the radar and the rotor target center, and β refers to the angle of pitch. Considering a 2-D slant-range plane, the simplified geometry is shown in Fig. 1(b), in which the radar coordinate system is established as XOY , and $X'O'Y'$ refers to the target coordinate system with the rotor target rotation center O' as the origin. The rotational radius of the scatterer P on the rotor blade is assumed as r , i.e., the distance from P to O' is r , and the distance from the radar to the scatterer P can be expressed as R_P . The rotational angular velocity of the scatterer P is denoted as ω , and the initial phase is denoted as θ_0 .



(a) Spatial geometry model



(b) 2-D plane geometry model

Fig. 1 Geometry model between the radar and the rotor target

According to the geometry model, the instantaneous distance of OP can be represented as

$$R_P(t_m) = \sqrt{(R_C + R_x(t_m))^2 + R_y(t_m)^2} \quad (1)$$

where $R_x(t_m)$ and $R_y(t_m)$ are the abscissa and the ordinate of the scatterer P respectively, $t_m = mT_r$ is the slow time, m is the order number of the transmitted pulse and T_r refers to the pulse repetition period. Under the condition of the far field, (1) can be rewritten as

$$R_P(t_m) \approx R_C + R_x(t_m) = R_C + r \cos(\omega t_m + \theta_0). \quad (2)$$

Suppose there is the radar that transmits linear frequency modulation (LFM) signals, which can be expressed as

$$s_t(\hat{t}, t_m) = \text{rect}(\hat{t}/T_p) \exp(j2\pi(f_c t + \mu \hat{t}^2/2)) \quad (3)$$

where $\text{rect}(\cdot)$ is the rectangular window, T_p refers to the pulse width, f_c refers to the signal carrier frequency, μ is the chirp rate of the LFM signal, t refers to the total time, \hat{t} is the fast time, and $t = \hat{t} + t_m$. The echo signal of the scatterer P can be expressed as

$$\begin{aligned} s_r(\hat{t}, t_m) = & \sigma \text{rect}(t_m/T_a) \text{rect}((\hat{t} - 2R_P(t_m)/c)/T_p) \cdot \\ & \exp(j2\pi f_c(t - 2R_P(t_m)/c)) \cdot \\ & \exp(j\pi\mu(\hat{t} - 2R_P(t_m)/c)^2) \end{aligned} \quad (4)$$

where σ refers to the scattering coefficient of the scatterer P , T_a is the observation time, and c refers to the speed of light. The following expression can be obtained by pulse compression of the echo signal:

$$\begin{aligned} s_c = & \sigma T_p \sin c[B(\hat{t} - 2R_P(t_m)/c)] \text{rect}(t_m/T_a) \cdot \\ & \exp(-j4\pi R_C/\lambda) \exp(-j4\pi r \cos(\omega t_m + \theta_0)/\lambda) \end{aligned} \quad (5)$$

where B is the signal bandwidth, and λ is the wavelength. The Doppler frequency can be obtained by taking the derivative of the phase as

$$\begin{aligned} f_{\text{md}} = & \frac{1}{2\pi} \frac{d\phi}{dt_m} = \frac{1}{2\pi} \frac{d[-4\pi r \cos(\omega t_m + \theta_0)/\lambda]}{dt_m} = \\ & 2\omega r \sin(\omega t_m + \theta_0)/\lambda. \end{aligned} \quad (6)$$

According to the above formula, we can conclude that the Doppler frequency of the scatterer on the rotor blade takes the form of sine function and is related to the rotor target parameters of ω and r . We can also obtain the maximum of the Doppler frequency as

$$f_{\text{md-max}} = 2\omega r/\lambda. \quad (7)$$

In the next section, we will describe how to identify the number information of blades and the manoeuvre intention based on the micro-Doppler features.

2.2 Radar data pre-processing

In this paper, we consider and clarify three different manoeuvre intentions of a rotor target, such as rising, hovering and falling. As we know, the change trend of rotational angular velocity of the scatterer P varies with different manoeuvre intentions, and the maximum Doppler frequency also presents different forms. For example, the rotational angular velocity of the scatterer P in the rotor blade increases approximately linearly in the rising state. The instantaneous angular velocity can be defined as

$$\omega(t_m) = \omega_0 + at_m \quad (8)$$

where ω_0 is the rotational angular velocity of the scatter P at the initial observation time, a is the rotational angular acceleration, and $a > 0$ indicates that the rotational angular velocity increases with slow time and the rotor target is rising. By that analogy, $a = 0$ and $a < 0$ represent the manoeuvre intentions which are hovering and falling, respectively. Correspondingly, the maximum Doppler frequency of the scatterer P in the rotor blade can be rewritten as

$$f_{\text{md-max}} = 2(\omega_0 + at_m)l/\lambda \quad (9)$$

where l refers to the rotor blade length.

Especially, we may change the manoeuvre intention through changing the propeller pitch and keeping a constant angular velocity. However, if the rotational angular velocity of the scatterer P in the rotor blade keeps unchanged and the rotor target is on the rising or falling state by changing the propeller pitch, the projection of the rotating radius of the scatterer P on the radar line of sight will also change, and then the sinusoidal time-frequency chart with a constant frequency and amplitude cannot be obtained. In addition, in this case, the rotor target will have a horizontal thrust and radial motion. We can classify the manoeuvre intentions by measuring the change of the radial distance.

As a typical algorithm of linear time-frequency transform, the STFT has received more and more attention, which clearly describes the relationship between the signal frequency and the time variation and can be expressed as

$$S[m, k] = \text{STFT}\{s[n]\} = \sum_{n=-\infty}^{+\infty} s[n]w[n-m] \exp(-j2\pi nk/N) \quad (10)$$

where $n = 1, 2, \dots, N - 1$, $S[m, k]$ refers to the result of the STFT of the signal $s[n]$, $s[n]$ refers to the discrete echo signal in the distance unit of the rotor target, and $w[n]$ denotes the discrete window function which is usually a Gaussian function, N refers to the size of the window function, k refers to the sampling point of discrete Doppler frequency, and $k = Nf/f_s$, where f refers to the discrete Doppler frequency, and f_s refers to the sampling frequency.

Fig. 2(a)–Fig. 2(c) plot the spectrograms of three manoeuvre intentions under the signal-to-noise ratio (SNR) of -10 dB. The simulation parameters of the transmitting signal and rotor target are shown as follows. Assume that there are four blades in the rotor target with the rotor blade length of 6 m, the fuselage of the rotor target consists of four scatterers, and the rotational angular velocity of the rotating parts is 4 r/s in the state of hovering.

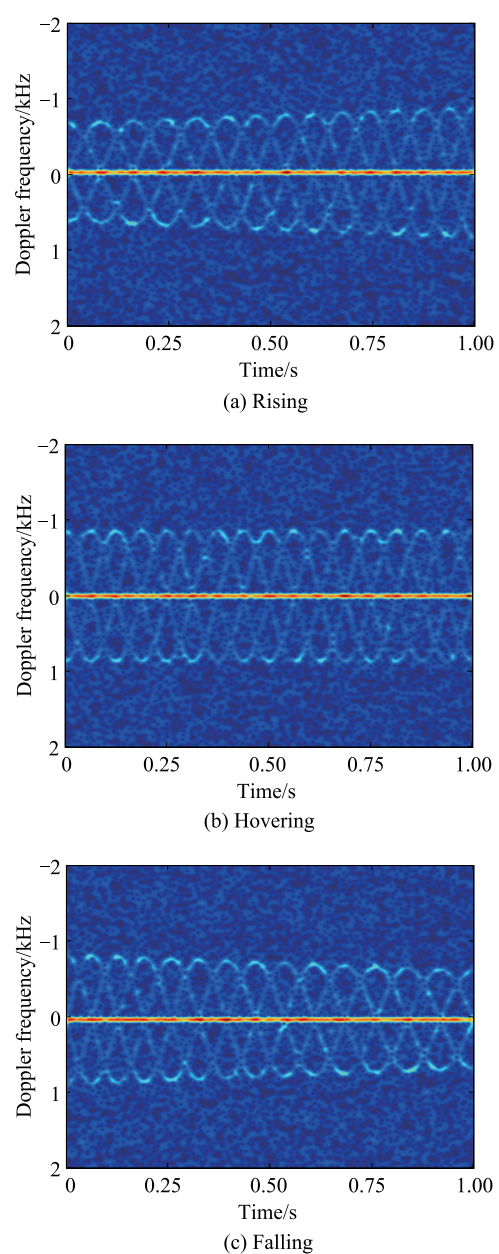


Fig. 2 Spectrograms under three manoeuvre intentions

The pulse repetition period T_r is 0.25 ms, the pulse width T_p is 50 μ s, the observation time T_a is 1 s, the bandwidth B of the LFM signal is 1 MHz and the carrier frequency f_c is 1 GHz.

3. The proposed algorithm

3.1 CNN architecture

A CNN architecture with seven layers is built to extract information from time-frequency spectrograms for parity recognition of blade number and manoeuvre intention classification of the rotor target, as shown in Fig. 3. As we can see from the CNN architecture model, the numbers fol-

lowed by “@” refer to the size of each feature map, and the numbers followed by “#” represent the parameters of the convolutional kernel, where the first three numbers refer to the size and the last number is the kernel depth. It comprises three CLs, two DSLs, and two FCLs. First, to reduce the computational complexity, the spectrogram inputs of the CNN architecture are down-sampled to 250×250 pixels. Although the image size is compressed, it still contains enough information for recognition and classification. Second, the features represented by the variation of the micro-Doppler frequency are extracted by CLs of the architecture. Finally, the vector reshaped after C5 is fed into two FCLs (Fc6 and Fc7) to produce the final output.

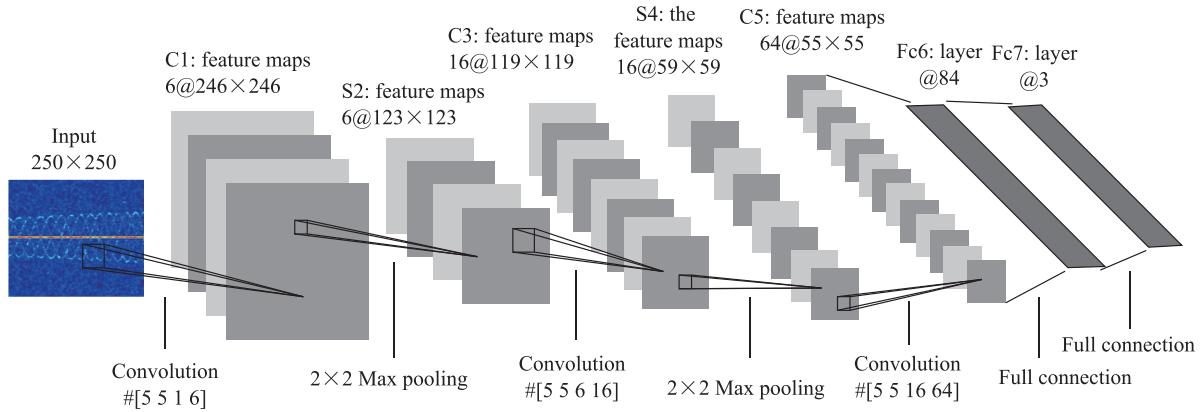


Fig. 3 CNN architecture

3.2 Training details

In this paper, the constructed CNN architecture is implemented by Tensorflow. To accelerate the convergence of the architecture and avoid over-fitting, we utilize batch processing and the dropout method when the architecture is trained, respectively. According to our several trials, it can be found that the architecture has the best ability to recognize and clarify the rotor target with the learning rate of 0.001 (training data ratio of 20%) and 0.002 (training data ratio of 50%) and with a size of 10 in batch processing.

To verify the effectiveness of the constructed CNN architecture, we partition the spectrograms of the datasets into three different radios of 20%, 33% and 50%. The datasets are divided randomly and evenly into five folds when the training data radio is 20%, and a fivefold cross validation method is used to acquire a stable and universal recognition and classification accuracy. In the same way, triple and double cross validations are respectively conducted in terms of 33% and 50% training data radios.

4. Simulation results

4.1 Randomly divided datasets

We first validate the manoeuvre intention classification of

the rotor target and the parity recognition performance of the blade number by the randomly divided training data radio mentioned above. Assume that there are two types of the rotor blades in the experiment, the blade numbers are two and three, respectively. The distance between the scatterer and the scatterer center on the rotor blade ranges from 4 m to 8 m, which contains 15 kinds of simulation data. The angular velocity of the rotor blade is simulated with 10 data in each manoeuvre intention, which ranges from 2 r/s to 6 r/s. Generally speaking, there are three manoeuvre intentions of the rotor target, and the number of samples for each state is 300. Table 1 shows the maximum, minimum and average accuracies for manoeuvre intentions classification and parity recognition of the blade number after the cross validation at SNR = 0 dB. As shown in Table 1, we can conclude that with an increasing training data ratio, the recognition accuracy of parity and manoeuvre intention is obviously improved at the same SNR. We also find that the manoeuvre intention classification accuracy is high enough and can reach 93.34% on average in terms of the 20% training data ratio, and the parity recognition of the blade number accuracy reaches 89.34% on average and 92% at maximum in terms of the 50% training data ratio.

Table 1 Parity recognition of blade number and manoeuvre intention classification accuracy

Accuracy	Parity recognition of blade number			Manoeuvre intention classification			
				Max.	Min.	Average	
	Max.	Min.	Average	Max.	Min.	Average	
Training data ratio	20	87.08	75.42	83.17	95.00	91.39	93.34
33	89.83	83.50	87.11	96.83	93.67	95.33	
50	92.00	86.67	89.34	99.11	97.34	98.23	

4.2 Training data ratio of 33%

To investigate the manoeuvre intention classification performance of this proposed algorithm under different SNRs, the time-frequency spectrograms with the training data ratio of 33% are input to the constructed CNN architecture for training. In this experiment, the datasets are the same as those in Section 4.1; we divide the datasets into three folds randomly and utilize the triple cross validation method. The classification accuracy is shown in Fig. 4, from which we can conclude that as the model training iterations increase, the classification accuracy of the triple cross validation improves and eventually reaches a steady state. We also conclude that the classification accuracy when SNR is 0 dB is higher than that when the SNR is -5 dB.

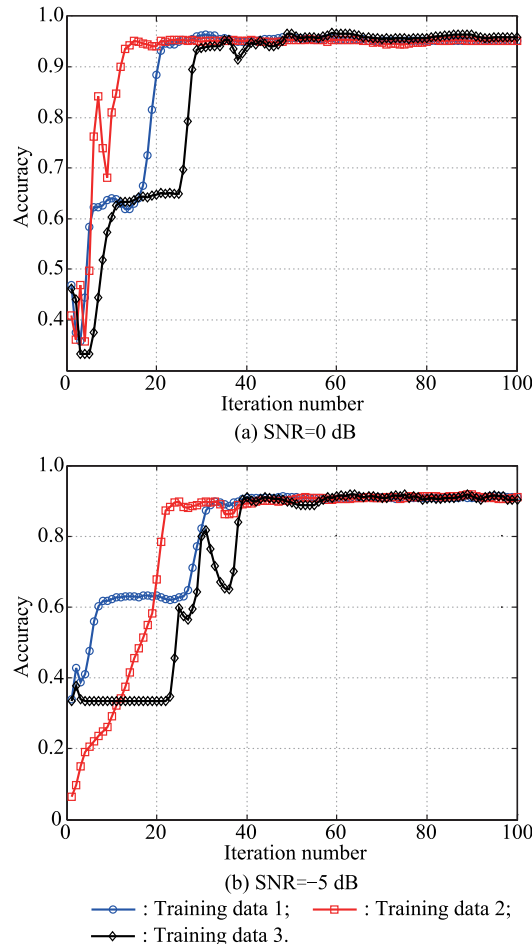


Fig. 4 Manoeuvre intention classification accuracy

Fig. 5 shows the manoeuvre intention classification performance under different SNRs from -10 dB to 3 dB. The maximum, minimum and average classification accuracies are given under each SNR. With the improvement of SNR, the average accuracy increases gradually and reaches 97.17% when SNR = 3 dB.

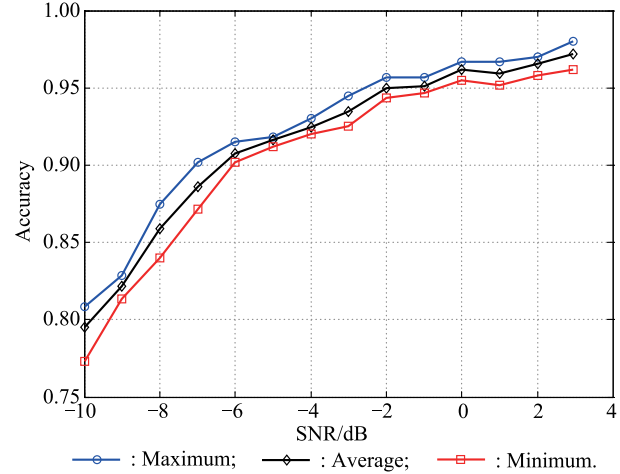


Fig. 5 Manoeuvre intention classification accuracy under different SNRs

5. Conclusions

A CNN architecture with seven layers is proposed based on micro-Doppler features for parity recognition of the blade number and manoeuvre intention classification of a rotor target. The spectrograms obtained by the STFT are divided into different folds and put into the constructed CNN model. The corresponding cross validation method is used to validate the effectiveness of the constructed CNN architecture. Simulation results show that, as the training data ratio increases, the parity recognition performance of the blade number and manoeuvre intention classification is all improved under the same SNR. The classification accuracy of manoeuvre intentions can reach 93.34% on average in terms of the training data ratio of 20% and reach over 98% on average in terms of the training data ratio of 50% when the SNR is 0 dB because the spectrograms obtained from the STFT of a rotor target with different manoeuvre intentions have different micro-Doppler features. In the experiment with different SNRs, the manoeuvre intention classification accuracy on average increases gradually from 79.50% at SNR = -10 dB to 97.17% at SNR = 3 dB. Measured radar data will be collected to verify the effectiveness of the constructed CNN architecture and the proposed algorithm in the future.

References

- [1] TU S, SU Y, WANG W. Automatic target recognition scheme

- for a high-resolution and large-scale synthetic aperture radar image. *Journal of Applied Remote Sensing*, 2015, 9(1): 096039.
- [2] LI B Q, HU X H. Effective distributed convolutional neural network architecture for remote sensing images target classification with a pre-training approach. *Journal of Systems Engineering and Electronics*, 2019, 30(2): 238–244.
- [3] CHEN Y, ZHANG Q, MA C. Micro motion feature extraction of radar target using tracking pulses with adaptive pulse repetition frequency adjustment. *Journal of Applied Remote Sensing*, 2014, 8(1): 083569.
- [4] RITCHIE M, FIORANELLI F, BORRION H. Multistatic micro-Doppler radar feature extraction for classification of unloaded/loaded micro-drones. *IET Radar, Sonar & Navigation*, 2017, 11(1): 116–124.
- [5] HARMANNY R I A, WIT J J M D, CABIC G P. Radar micro-Doppler feature extraction using the spectrogram and the cepstrrogram. *Proc. of the European Radar Conference*, 2014: 165–168.
- [6] KIM B K, KANG H S, PARK S O. Drone classification using convolutional neural networks with merged Doppler images. *IEEE Geoscience and Remote Sensing Letters*, 2017, 14(1): 38–42.
- [7] BJORKLUND S, PETERSSON H, HENDEBY G. Features for micro-Doppler based activity classification. *IET Radar, Sonar & Navigation*, 2015, 9(9): 1181–1187.
- [8] DING J, CHEN B, LIU H. Convolutional neural network with data augmentation for SAR target recognition. *IEEE Geoscience and Remote Sensing Letters*, 2016, 13(3): 364–368.
- [9] DING B Y, WEN G J, HUANG X H. Data augmentation by multilevel reconstruction using attributed scattering center for SAR target recognition. *IEEE Geoscience and Remote Sensing Letters*, 2017, 16(4): 979–983.
- [10] ZHANG J, ZHAO H Z, FU Q, et al. Recognition of a hovering helicopter. *Systems Engineering and Electronics*, 2002, 24(2): 6–8. (in Chinese)
- [11] FENG X B, HUANG P K. Analysis of the spectrum signature of the radar return signal from aircraft rotating blades. *Systems Engineering and Electronics*, 2005, 27(3): 385–387. (in Chinese)
- [12] CHEN H Y, LI X, GUO G R, et al. Identification of air target based on the micro-motion radar signatures of blades. *Systems Engineering and Electronics*, 2006, 28(3): 372–375. (in Chinese)
- [13] ZHANG C S, WANG P Y, CHEN K, et al. Identify-aware convolutional neural network for facial expression recognition. *Journal of Systems Engineering and Electronics*, 2017, 28(4): 784–792.
- [14] KIM Y, TOOMAJIAN B. Hand gesture recognition using micro-Doppler signatures with convolutional neural network. *IEEE Access*, 2016, 4: 7125–7130.
- [15] XIA J F, YANG X Z, JIA L. A multi-depth convolutional neural network for SAR image classification. *Remote Sensing Letters*, 2018, 9(12): 1138–1147.
- [16] YANG L, CHEN G, LI G. Classification of personnel targets with baggage using dual-band radar. *Remote Sensing*, 2017, 9(6): 594.
- [17] ZHONG Y, FENG F, ZHANG L. Large patch convolutional neural networks for the scene classification of high spatial resolution imagery. *Journal of Applied Remote Sensing*, 2016, 10(2): 025006.
- [18] CHEN Z X, LI G, FIORANELLI F. Personnel recognition and gait classification based on multistatic micro-Doppler signatures using deep convolutional neural networks. *IEEE Geoscience and Remote Sensing Letters*, 2018, 15(5): 669–673.
- [19] WANG J, WANG Y H, LIU H W, et al. Polarimetric SAR image change detection based on deep convolutional neural network. *Systems Engineering and Electronics*, 2018, 40(7): 1457–1463. (in Chinese)
- [20] LEE H, KWON H. Going deeper with contextual CNN for hyperspectral image classification. *IEEE Trans. on Image Processing*, 2017, 26(10): 4843–4854.
- [21] KIM Y, MOON T. Human detection and activity classification based on micro-Doppler signatures using deep convolutional neural networks. *IEEE Geoscience and Remote Sensing Letters*, 2016, 13(1): 8–12.
- [22] YIN Q B, SHEN L R, LU M Y, et al. Selection of optimal window length using STFT for quantitative SNR analysis of LFM signal. *Journal of Systems Engineering and Electronics*, 2013, 24(1): 26–35.

Biographies



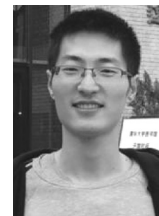
WANG Wantian was born in 1992. He received his B.E. and M.S. degrees in radar engineering and information and communication engineering from Air Force Early Warning Academy in 2015 and 2017, respectively. He is currently pursuing his Ph.D. degree in Air Force Early Warning Academy. His current research interests include radar signal processing and target classification and recognition.

E-mail: laodifang0120@126.com



TANG Ziyue was born in 1966. He received his M.S. and Ph.D. degrees from Air Force Early Warning Academy and Naval Engineering University, Wuhan, China in 1990 and 2000, respectively. He is currently a professor of Air Force Early Warning Academy. His current research interests include radarsignal processing, anti-interference, target detection and imaging, and radar automatic target recognition.

E-mail: tang_zi_yue@163.com



CHEN Yichang was born in 1988. He received his M.S. and Ph.D. degrees in electronic engineering from the Institute of Information and Navigation, Air Force Engineering University, Xi'an, China in 2013 and 2017, respectively. From 2014 to 2017, he was a visiting scholar at Tsinghua University, Beijing, China. Since 2018, he has been with the faculty of Air Force Early Warning Academy, China, where he is currently a lecturer. His current research interests include radar imaging, compressed sensing and radar automatic target recognition.

E-mail: cyc_2007@163.com



SUN Yongjian was born in 1976. He received his Ph.D. degree in the Second Academy of China Aerospace Science and Industry Co. Ltd., Beijing, China, in 2014. He is currently an instructor in Air Force Early Warning Academy. His current research interests include compressive sensing, radar signal processing and AI based automatic target recognition.

E-mail: bmdsun@126.com